

Full length article

Carbon monoxide degassing from seismic fault zones in the Basin and Range province, west of Beijing, China

Yutao Sun^{a,b}, Xiaocheng Zhou^c, Guodong Zheng^d, Jing Li^e, Hongyu Shi^c, Zhengfu Guo^{a,*}, Jianguo Du^{e,c,*}^a Key Laboratory of Cenozoic Geology and Environment, Institute of Geology and Geophysics, Chinese Academy of Sciences, Beijing 100029, China^b University of Chinese Academy of Sciences, Beijing 100049, China^c CEA Key Laboratory of Earthquake Prediction (Institute of Earthquake Science), China Earthquake Administration, Beijing 100036, China^d Key Laboratory of Petroleum Resources, Gansu Province/Key Lab of Petroleum Resources Research, Institute of Geology and Geophysics, Chinese Academy of Sciences, Lanzhou 730000, China^e Institute of Disaster Prevention, Yanjiao, Hebei Province 065201, China

ARTICLE INFO

Keywords:

Carbon monoxide
Degassing
Flux
Active fault zone
BRPB

ABSTRACT

Degassing of carbon monoxide (CO), which plays a significant role in the contribution of deep carbon to the atmosphere, commonly occurs within active fault zones. CO degassing from soil to the atmosphere in the Basin and Range province, west of Beijing (BRPB), China, was investigated by in-situ field measurements in the active fault zones. The measured concentrations of CO in soil gas in the BRPB ranged from 0.29×10^{-6} to 1.1×10^{-6} with a mean value of 0.6×10^{-6} , which is approximately twice as large as that in the atmosphere. Net fluxes of CO degassing ranged from $-48.6 \text{ mg m}^{-2} \text{ d}^{-1}$ to $12.03 \text{ mg m}^{-2} \text{ d}^{-1}$. The diffusion of CO from soil to the atmosphere in the BRPB was estimated to be at least $7.6 \times 10^3 \text{ ton/a}$, which is comparable to the corresponding result of about $1.2 \times 10^4 \text{ ton/a}$ for CO_2 . CO concentrations were spatially heterogeneous with clearly higher concentrations along the NE-SW trending in the BRPB. These elevated values of CO concentrations were also coincident with the region with low-velocity and high conductivity in deep mantle, and high Poisson's ratio in the crust, thereby suggesting that CO degassing from the soil might be linked to upwelling of the asthenospheric mantle. Other sources of CO in the soil gas are suggested to be dominated by chemical reactions between deep fluids and carbonate minerals (e.g., dolomite, limestone, and siderite) in country rocks. Biogenic processes may also contribute to the CO in soil gas. The spatial distribution patterns of CO concentrations are coincident with the stress field, suggesting that the concentrations of CO could be a potential indicator for crustal stress field and, hence is potential useful for earthquake monitoring in the BRPB.

1. Introduction

Carbon monoxide (CO), an important gaseous component of the troposphere, plays a significant role in the Earth's carbon cycle (Crutzen and Zimmermann, 1991; Novelli et al., 1992; Badr and Probert, 1994; Kasischke et al., 2005). As a consequence of its warming potential, which is approximately 1.4 times greater than that of CO_2 (Lashof and Ahuja, 1990), CO has been taken as a precursor and an indirect source of the greenhouse effect by the Intergovernmental Panel on Climate Change (IPCC) (Prather et al., 2001; Gillenwater et al., 2006). Anomalous concentrations of CO in the atmosphere are generally related to earthquake activity, as revealed by high spectral resolution remote

sensing satellite data (e.g., Singh et al., 2010; Cui et al., 2013; Sun et al., 2014). However, the origin, concentration and flux of CO degassing from soil along the active fault zones remain poorly understood.

Many active faults have been identified in the Basin and Range province in the west of Beijing (BRPB), which is an area characterized by strong Neotectonic activity and with a high potential for earthquakes (Fig. 1b, Xu and Ma, 1992). It has been selected by the Chinese Earthquake Administration as a prime seismic monitoring area in China. In this paper we discuss output of CO degassing diffusion from the active fault zones in the BRPB and a possible link between CO emission and fault activity.

* Corresponding authors at: No. 19, Beitucheng Western Road, Chaoyang District, Beijing 100029, China (Z. Guo), Institute of Disaster Prevention, Yanjiao, Hebei Province 065201, China (J. Du).

E-mail addresses: zfguo@mail.iggcas.ac.cn (Z. Guo), jianguodu@hotmail.com (J. Du).

<http://dx.doi.org/10.1016/j.jseaes.2017.07.054>

Received 1 August 2016; Received in revised form 27 July 2017; Accepted 27 July 2017

Available online 29 July 2017

1367-9120/ © 2017 Elsevier Ltd. All rights reserved.

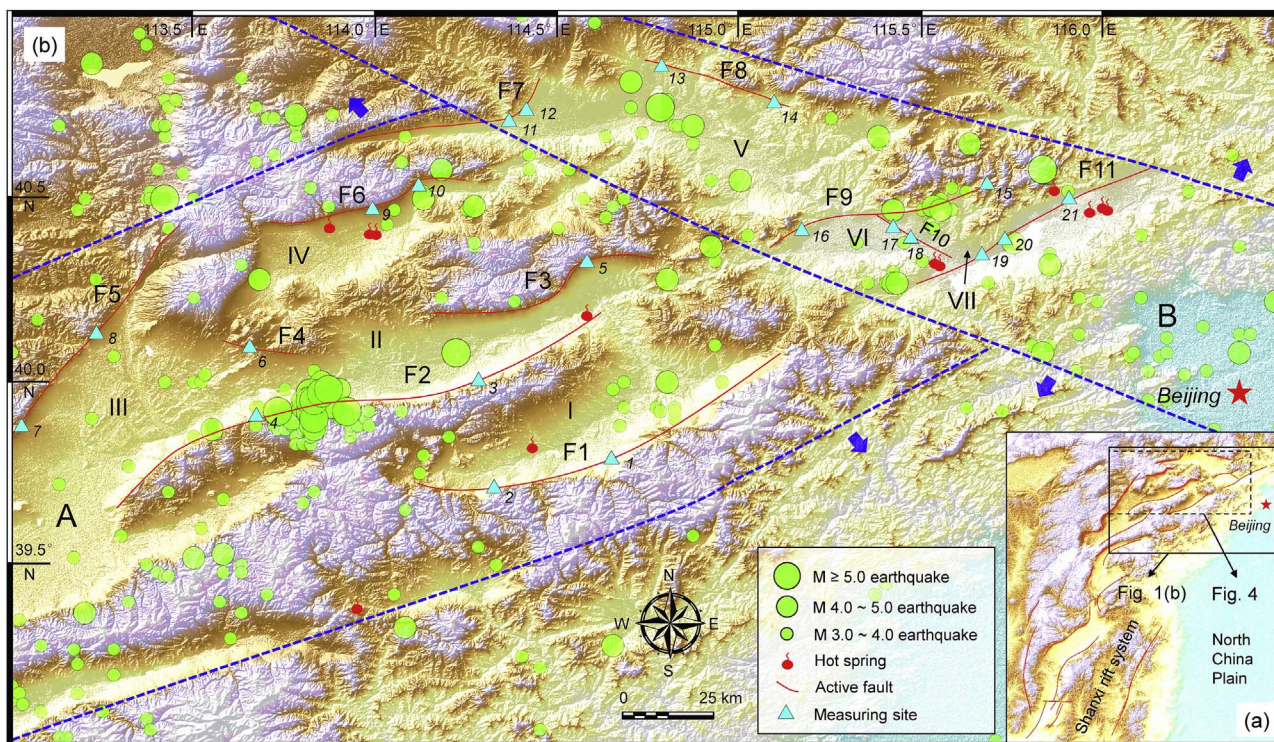


Fig. 1. Topographic map showing active faults and measuring sites in the BRPB. (a) Location of the studied area. Rectangles of black solid lines show the regions in Figs. 1(b) and 4, respectively. (b) Distributions of active faults and measuring sites. Solid thick blue arrows showing stress field (Zhang et al., 2009a). Regions outlined by blue dashed lines are the Shanxi and Zhangjiakou-Bohai seismic zones, which are labelled as A and B, respectively (modified after Zhang et al., 2009a and Gao et al., 2011). Basins and active faults are labelled by the following letters: I, Yuguang Basin; II, Yangyuan Basin; III, Datong Basin; IV, Yanggao-Tianzhen Basin; V, Huaian Basin; VI, Huaizhuo Basin; VII, Yanfan Basin; F1, Yuguang Basin south-margin fault; F2, Liulengshan fault; F3, Yangyuan Basin north-margin fault; F4, Datong volcano fault; F5, Kouquan fault; F6, Yanggao-Tianzhen fault; F7, Huaian Basin north-margin fault; F8, Zhangjiakou fault; F9, Huaizhuo Basin north-margin fault; F10, Xinbaoan-Shacheng fault; F11, Yanfan Basin north-margin fault. Numbers and abbreviations of the measuring sites are as follows: 1, Beikou (BKC); 2, Yixingzhuang (YXZ); 3, Yanjiayao (YJY); 4, Donghouzi (DHZ); 5, Nankoucun (NKC); 6, Datong volcano (DTV); 7, Shijingcun (SJC); 8, Shanghuangzhuang (SHZ); 9, Yulinkou (YLK); 10, Zhangzhongkou (ZZK); 11, Yangjiaogou (YJG); 12, Niujiaoyao (NJY); 13, Wanquanxian (WQX); 14, Qingbiankou (QBK); 15, Xihongzhan (XHZ); 16, Haojiapo (HJP); 17, Dongyuanzi (DYZ); 18, Liangtiantun (LTT); 19, Bayingcun (BYC); 20, Canfangying (CFY); 21, Yuhuangmiao (YHM). (For interpretation of the references to colour in this figure legend, the reader is referred to the web version of this article.)

2. Geological setting

The BRPB (39.0°–41.0°N, 113.0°–116.5°E) is tectonically situated on the north end of the Shanxi rift system (Fig. 1a, Xu and Ma, 1992; Huang and Zhao, 2004; Lu et al., 2008; Gao et al., 2011), which is one of the most significant Pliocene-Quaternary continental rift systems in China. A series of active faults in the rift system are oriented parallel to the continental margin of the Trans-North China Block (Fig. 1a). It is seismically highly active and subject to strong earthquakes (Xu et al., 2002; Li et al., 2015). The Shanxi and Zhangjiakou-Bohai seismic zones are located in the west and northeast of the BRPB, respectively (Fig. 1b). The active faults in the BRPB can be classified into two groups based on their strikes: one group trends NNE to NE and the other NNW to NW (Fig. 1b). The first group includes the Yuguang Basin south-margin fault (F1), the Liulengshan fault (F2), the Yangyuan Basin north-margin fault (F3), the Kouquan fault (F5), the Yanggao-Tianzhen fault (F6), the Huaian Basin north-margin fault (F7), the Huaizhuo Basin north-margin fault (F9) and the Yanfan Basin north-margin fault (F11). The second group mainly includes the Datong volcano fault (F4), the Zhangjiakou fault (F8) and the Xinbaoan-Shacheng fault (F10) (Fig. 1b, Zhang et al., 2009a). The BRPB hosts numerous hot springs on the alluvial fans and in the fault zones (Fig. 1b, Zhang et al., 2016). Those hot springs furnish abundant degassing sites, many of which may degas continuously.

The BRPB has an Archean to Paleoproterozoic metamorphosed basement, with an unmetamorphosed cover of Mesoproterozoic to Phanerozoic sedimentary rocks (Lu et al., 2008; Zhang et al., 2009b). The basement is mainly composed of Neoproterozoic tonalite-trondhjemitic-granodioritic (TTG) gneisses, mafic dikes and syn- or post-syn-tectonic granites (Lu et al., 2008). Following the final amalgamation of

the Eastern and Western Blocks along the trans-North China Orogen at approximately 1.8 Ga, the North China Craton was covered by thick sequences of Meso-Neoproterozoic rocks of the unmetamorphosed Changcheng, Jixian and Qingbaikou Systems and by Cambrian-Ordovician marine clastic and carbonate platformal sediments (Lu et al., 2008; Zhang et al., 2009b). Detailed information and geological characteristics of the strata have been described in Lu et al. (2008) and Zhang et al. (2009b). The surface lithology in the BRPB is dominated by limestones and sandstones, which are the source rocks of the Quaternary unconsolidated sediments in the basins (Zhang et al., 2016).

3. Method and data processing

3.1. Measurement method

The concentration and flux of CO in soil gas were measured in the BRPB in May 2014. CO concentrations in soil gas were measured at 269 points on 21 sites crossing 11 major faults (Fig. 1b and Table 1). Survey lines with 10 measuring points at 20 m intervals were laid out at each site. Closer spacing, with 4 survey lines at 5 m intervals, was laid out at the Liangtiantun (LTT) and Dongyuanzi (DYZ) sites on the Xinbaoan-Shacheng fault (F10) (Fig. 1b), which has been regularly active throughout the Holocene (Xu et al., 2002).

Concentrations of CO in soil gas were measured using the method of Zhou et al. (2015) and Li et al. (2013) (Fig. 2a). Flux of CO degassing was measured with a closed-chamber (Fig. 2b) as described by Chiodini et al. (1998), Nakano et al. (2004), and Zhou et al. (2015). Concentration and flux of CO in soil gas were both measured using the GXH

Table 1
CO degassing fluxes along the fault in the BRPB.

Seismic zone	Fault	n	N	$C_f (\times 10^{-6})$	$C_{iMax} (\times 10^{-6})$	C value	Degassing flux ($\text{mg m}^{-2} \text{d}^{-1}$)	$T_{soil} (\text{°C})$
A	F1	20	2	0.55	2.40	4.36	18.05	30.2
	F2	20	2	0.60	1.30	2.18	6.80	28.8
	F3	10	1	0.82	2.40	2.93	10.62	32.0
	F4	10	1	0.57	0.70	1.22	6.71	22.0
	F5	20	2	0.29	0.70	2.46	4.81	23.6
	F6	20	2	0.50	1.10	2.20	0.80	23.1
B	F7	20	2	0.43	0.80	1.86	30.59	29.0
	F8	20	2	0.37	1.00	2.74	3.05	28.5
	F9	20	2	1.10	9.80	8.95	7.16	27.0
	F10	80	2	0.69	2.40	3.48	n.p.	27.3
	F11	29	3	0.38	2.30	6.05	8.35	27.8

A and B represent the Shanxi seismic zone and Zhangjiakou-Bohai seismic zone, respectively. Abbreviation of each fault (from F1 to F11) corresponds to that in Fig. 1(b). Letters of “n” and “N” are the numbers of measuring points and measuring sites at each fault, respectively. C_f and C_{iMax} are the mean and maximum values of CO concentrations in soil gas at each fault, respectively. $C \text{ value} = C_{iMax}/C_f$. n.p. = no positive value.

3011-A CO Analyzer with a measuring range of $0\text{--}50 \times 10^{-6}$, resolution of 0.1×10^{-6} , and accuracy of 4% of the reading. The analytical principle of the apparatus is Non-Dispersive Infrared (NDIR), based on gas filter correlation. Initial energy transmitted from the infrared source (I_0) is absorbed by the CO gas when it passes through the multi-reflection gas chamber of length L . The ultimate energy (I) is then measured by the infrared detector (Fig. 2c). CO concentration is calculated in accordance with the Lambert-Beer’s Law with the equation $I = I_0 e^{-KCL}$, where K and C are the infrared absorption coefficient and CO concentration, respectively (Xu and Chen, 2012).

3.2. Data processing

The mean value of CO concentration in each fault (C_f) was determined by the mean value of the CO concentration at all measuring

points (C_i) along the fault. The intensity of CO concentration of each fault was described using the contrast value (C), expressed by Eq. (1).

$$C = C_{iMax}/C_f \tag{1}$$

where C_{iMax} is the maximum value of C_i at each site.

The background value of CO concentration in soil gas of the BRPB was the mean value of CO concentrations of all measuring points after eliminating anomalous values. Anomalous values were determined by the anomalous threshold, which was calculated using the Quantile-Quantile plot (Q-Q plot) method (Sinclair, 1991; Zhou et al., 2010). This method can distinguish the anomalous values with an objective approach to statistical anomaly threshold estimation (Sinclair, 1991; Zhou et al., 2010; Voltattorni et al., 2014). The anomalous values of CO concentrations in soil gas were those that were less than the lower anomalous threshold and higher than the upper anomalous threshold.

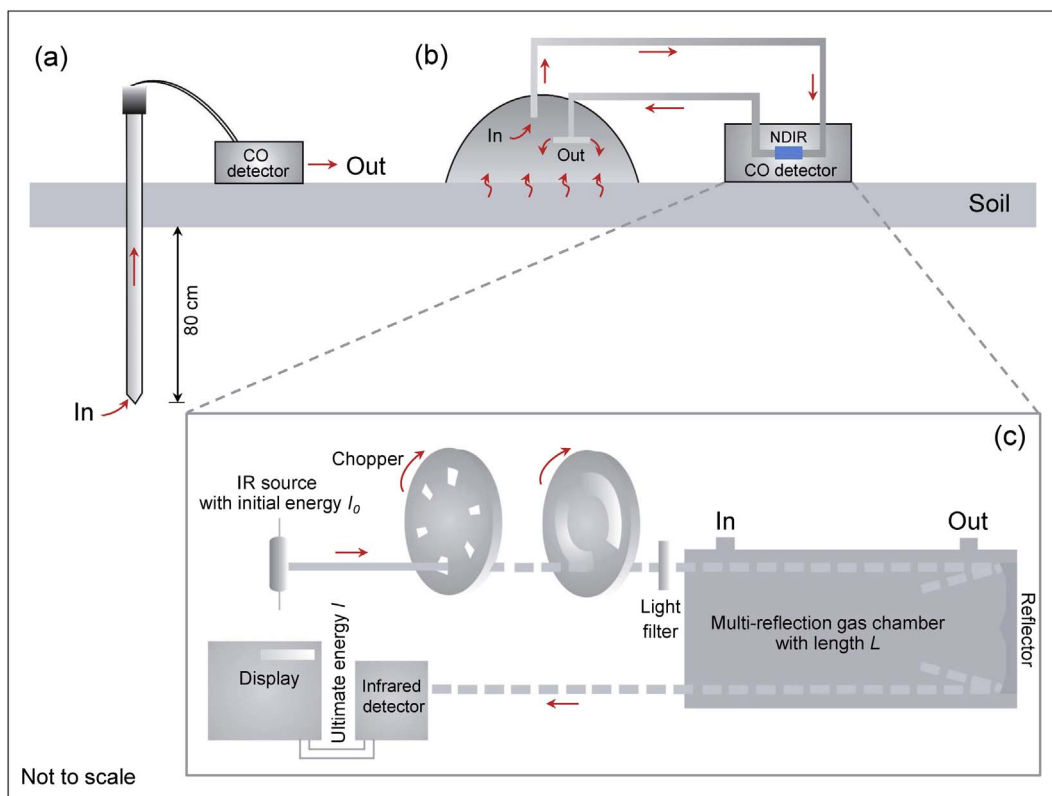


Fig. 2. Sketches of measurement methods for CO concentration (a) and flux (b) and analytical principle of the apparatus (c) (see text for details).

Flux of CO in soil gas was calculated based on the accumulation of CO concentration in the closed-chamber with time (Chiodini et al., 1998; Nakano et al., 2004), which was represented by Eq. (2).

$$F_{CO} = \frac{\rho_{CO} \cdot V_{chamber} \cdot P_{chamber} \cdot T_{standard} \cdot \frac{dc}{dt}}{P_{standard} \cdot T_{chamber} \cdot A_{chamber}} \quad (2)$$

where F_{CO} is the CO flux ($\text{g m}^{-2} \text{d}^{-1}$), and ρ_{CO} is the density of CO (1.25 kg/m^3) at standard temperature and pressure (STP). V (m^3) and A (m^2) are the volume and bottom area of the closed-chamber, respectively. $P_{chamber}$ and $T_{chamber}$ are the atmospheric pressure and temperature measured in the field, respectively. $P_{standard}$ and $T_{standard}$ represent the atmospheric pressure and temperature at STP, respectively. $\frac{dc}{dt}$ is the initial slope of curve of CO concentration with respect to time in the closed-chamber.

4. Results

4.1. Concentration of CO in soil gas

Concentration of CO in soil gas at each fault (C_p) varied between 0.29×10^{-6} and 1.1×10^{-6} (Table 1). The maximum value of CO concentration ($C_{iMax} = 9.8 \times 10^{-6}$) and the maximum contrast value ($C = 8.95$) were on F9 in the eastern part of the research region (Table 1 and Fig. 4). The upper and lower anomalous thresholds of CO concentrations in soil gas were 1.2×10^{-6} and 0.3×10^{-6} , respectively (Fig. 3). After ruling out the anomalous values, the background value of CO concentration in soil gas in the BRPB was 0.6×10^{-6} , which is approximately twice as large as the CO concentration in the atmosphere (0.3×10^{-6} , Novelli et al., 1992).

High values of CO concentrations in soil gas were appeared along the NE-SW trending in the BRPB (Fig. 4). The most significant CO concentration anomalies occurred at F9, F10, and F11 in the north-eastern part of the study area; significant anomalies occurred at F1, F2, and F3 in the central part (Table 1). CO concentrations along survey lines 1, 3, and 4 at LTT site showed a bimodal pattern across the fault (Fig. 5a), while those along survey line 2 at LTT site (Fig. 5a) and survey lines 1–4 at DYZ site (Fig. 5b) showed unimodal pattern. Such spatial distributions of CO concentrations in soil gas across the fault can be attributed to variations of permeability structures in the fault, which is composed of a coarse-grained breccia zone. It functions as a conduit

for fluid flow and a fine granular fault core that acts as a seal (Agosta et al., 2007). The strata in the LTT site are composed of a clay loam and sand-gravel layer. The clay loam in the core of the fault has low permeability (Ran, 1997), which obstructs gas migration. While at the DYZ site, by contrast, the core of the fault is sand-gravel (Ran, 1997), which facilitates the migration of gas.

4.2. Flux of CO diffusion

The measured fluxes and the estimated output of CO in the BRPB are shown in Table 2. Positive values of CO fluxes ('degassing flux') represent the diffusion of CO from soil into the atmosphere, while negative values ('uptake flux') represent CO uptake from atmosphere into soil. The degassing and uptake fluxes of CO in the BRPB varied in the ranges of $0.80\text{--}18.05 \text{ mg m}^{-2} \text{d}^{-1}$ and $-52.18 \text{ mg m}^{-2} \text{d}^{-1}$ to $-6.02 \text{ mg m}^{-2} \text{d}^{-1}$, respectively (Table 2). Considering synthetic actions of degassing and uptake of CO from the soil, net fluxes of CO in the BRPB ranged from $-48.6 \text{ mg m}^{-2} \text{d}^{-1}$ to $12.03 \text{ mg m}^{-2} \text{d}^{-1}$ (Table 2). The total output of CO in the active fault zones was $7.6 \times 10^3 \text{ ton/a}$ (Table 2). According to the IPCC Guidelines for Greenhouse Gas Inventories for CO gas (Eq. (3), Gillenwater et al., 2006), the diffusion of CO from the fault zones in the BRPB could therefore be estimated as equivalent to that of about $1.2 \times 10^4 \text{ ton/a}$ of CO_2 .

$$\text{Inputs}_{\text{CO}_2} = \text{Diffusions}_{\text{CO}} \cdot 44/28 \quad (3)$$

5. Discussion

5.1. Potential sources of CO in soil gas

Possible processes accounting for formation of CO in soil gas might include biogenic processes (Conrad and Seiler, 1980, 1982; Conrad and Thauer, 1983; Khalil et al., 1990; Funk et al., 1994; Elio et al., 2016), degassing from the inner Earth (Trump and Miller, 1973; Elio et al., 2016) and chemical reactions involving degassed CH_4 , H_2 , CO_2 , etc. (Schlesinger, 1999; Gødde et al., 2000; Etiopie and Lollar, 2013; Elio et al., 2016). The emission of CO in soil by disintegration of organic matter depends on soil temperature (Conrad and Seiler, 1982; Yonemura et al., 2000). Data from the BRPB (Table 1) showed presence of the positive correlation between soil temperature and CO degassing fluxes ($r = 0.48$), which indicated a biogenic contribution to the soil gas most probably produced by microbial oxidation of soil-derived carbon (Conrad and Seiler, 1980, 1982). In the BRPB, the CO fluxes from soil to atmosphere ranged from $0.8 \text{ mg m}^{-2} \text{d}^{-1}$ to $18.05 \text{ mg m}^{-2} \text{d}^{-1}$ (Table 2), which were much larger than those from the biogenic CO fluxes in soil (e.g., $1.1 \text{ mg m}^{-2} \text{d}^{-1}$ and $3\text{--}4 \text{ mg m}^{-2} \text{d}^{-1}$, Funk et al., 1994; Constant et al., 2008). It can thus be deduced that the abiotic processes may contribute to the CO in soil gas in the BRPB.

The C-H-O fluids (e.g., H_2 , CH_4 , CO , CO_2 , H_2O) are considered as critical C-bearing fluids in the crust and mantle (Taylor and Green, 1988; McCammon and Kopylova, 2004; Frost and McCammon, 2008; Zhang and Duan, 2009). The mantle and lower crust can be one of the important sources of CO (Bergman and Dubessy, 1984). Geophysical data have demonstrated prominent low-velocity anomalies and high-conductivity layers occur beneath the Zhangjiakou-Bohai seismic zone in the northeast and Shanxi seismic zone in the west (Fig. 1b), suggesting an upwelling of high temperature fluids from the local upper mantle (Huang and Zhao, 2004, 2006, 2009; Lei, 2012). P-wave velocity tomography indicates a prominent low-velocity anomaly originating from the mantle transition zone and attaining the bottom of the crust in the BRPB (Tian et al., 2009; Santosh et al., 2010). The regions with high Poisson's ratios correspond to those with low-velocity anomalies and high conductivities thereby indicating an existence of fluids in the mantle-crust system (Wang et al., 2009). Spatial distributions of the high CO concentrations (Fig. 4) were found in the areas

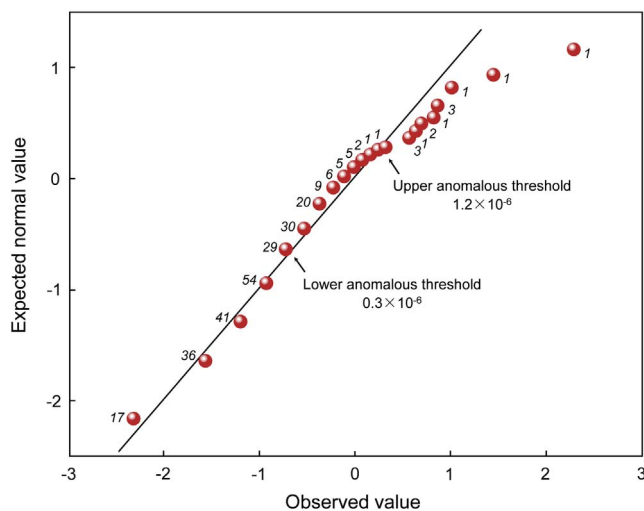


Fig. 3. Quantile-Quantile plot (Q-Q plot) showing the upper and lower boundary anomalous thresholds of CO concentrations in soil gas. Figures beside each red dot represent statistical number of the measuring points with the same CO concentration. (For interpretation of the references to colour in this figure legend, the reader is referred to the web version of this article.)

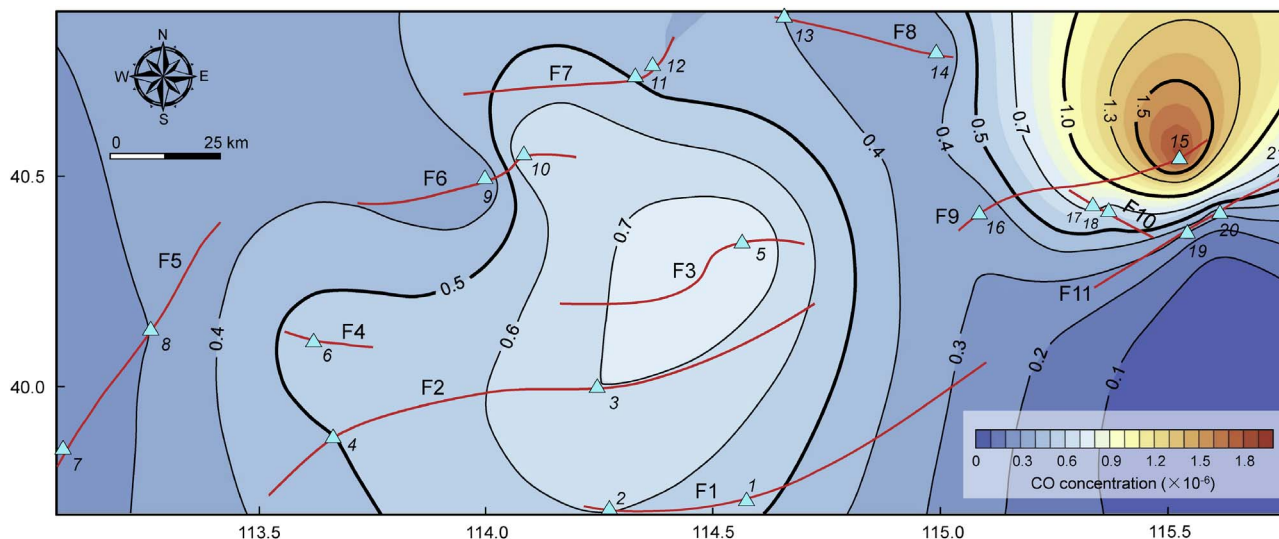


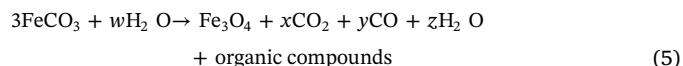
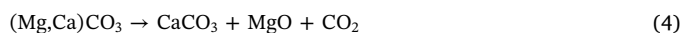
Fig. 4. Distribution of CO concentrations in soil gas. Cyan triangles and red solid lines are as in Fig. 1(b). (For interpretation of the references to colour in this figure legend, the reader is referred to the web version of this article.)

with low-velocity anomalies (Huang and Zhao, 2004, 2006, 2009; Lei, 2012) and high Poisson's ratios (Wang et al., 2009). Thermochemical calculations indicate that CH_4 production is most favored at 500 °C and < 7 GPa (Scott et al., 2004). Molecular dynamic simulations predict that the C-H-O fluids could be CH_4 -rich at greater depth. When the ascending fluids cross the boundary between lithosphere and asthenosphere, the reduced fluids enriched in $\text{H}_2\text{O}-\text{CH}_4-\text{H}_2$ will be oxidized into $\text{H}_2\text{O}-\text{CO}_2-\text{CO}$ fluids (Zhang and Duan, 2009). The presence of mantle-derived volatiles in the BRPB has been geochemically demonstrated by Zhang et al. (2016). Thus it might be inferred that degassing of the CO generation is associated with the upwelling of asthenospheric mantle. Crustal seismic velocity structure shows a presence of the deep faults in the BRPB, such as the Huailai-Lingqiu, Tianzhen, and Zhuolu-Yangyuan faults (Xu et al., 2002). These deep faults could penetrate to the uppermost mantle (Xu et al., 2002). There is a positive correlation ($r = 0.50$) between fault slip rate and $^3\text{He}/^4\text{He}$ ratio in the BRPB (Table 3). The $^3\text{He}/^4\text{He}$ ratio, as representative of overall fault-slip activity, is thought to be also related to fault permeability and to the transport of mantle volatiles (Zhang et al., 2016). The deep faults in the BRPB act as conduits for the migration of mantle-derived volatiles (e.g., H_2 , CH_4 , CO, CO_2 , H_2O) (Fig. 6a, Hilton, 2007; Zhang et al., 2016).

CO is expected to be a stable species in C-H-O system at high temperature and pressure conditions (Bergman and Dubessy, 1984; Zhang and Duan, 2009; Scott et al., 2004). The $^3\text{He}/^4\text{He}$ ratios in the crust and mantle are 0.02 R_a and 8 R_a , respectively (where R_a is the $^3\text{He}/^4\text{He}$ ratio in air, Lupton, 1983; Hilton et al., 2002). There is a negative correlation ($r = -0.54$) between CO concentration and $^3\text{He}/^4\text{He}$ ratio in the BRPB (Table 3), suggesting the upwelling of the asthenospheric mantle as

other source of CO in the BRPB.

The North China Craton is composed of Archean and Paleoproterozoic metamorphic basement overlain by approximately 9000 m of unmetamorphosed Mesoproterozoic sedimentary cover with prominent thick-layered dolomites and limestone (Lu et al., 2008; Zhang et al., 2009b). Siderite was also deposited in the Xiamaling Formation in the Neoproterozoic times (Zhang and Duan, 2009; Fan, 2015). The thermobarometry of Cenozoic basalt-borne peridotites reveals that the temperatures at lower crustal depth and in the sub-Moho mantle beneath the North China Craton are 750–1200 °C and 1200–1280 °C, respectively (Menzies et al., 2007). Heat input from the upwelling of the asthenospheric mantle and its interactions with overlying carbonates would lead to release of the CO_2 -rich fluids when the temperature attains at 500 °C (Fig. 6a, Sulem and Famin, 2009; Santosh et al., 2010). Thermal decomposition of the carbonate rocks (CaCO_3) and siderite (FeCO_3) might generate CO_2 and CO by Eqs. (4) and (5) (Fig. 6a, Gao, 1997; Treiman, 2003; McCollom, 2003; Etiopie and Lollar, 2013).



where w , x , y and z are undetermined stoichiometric coefficients (Treiman, 2003; McCollom, 2003; Etiopie and Lollar, 2013). CO might be generated by the chemical reactions among the $\text{CO}_2-\text{CH}_4-\text{H}_2-\text{H}_2\text{O}$ fluids and carbonate rocks (Eq. (6), Fig. 6a) and by the chemical reactions among the degassed volatiles (Eqs. (7)–(10), Fig. 6a and b,

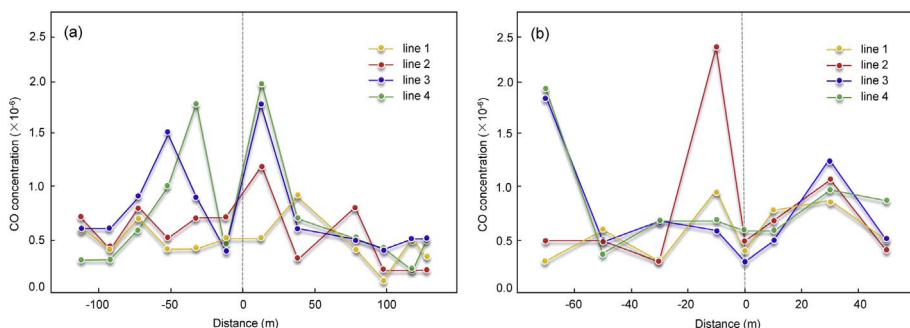


Fig. 5. Plots of CO concentration versus distance from F10 at LTT site (a) and DYZ site (b). Grey dashed lines show location of the fault. The abscissa values show distances from measuring point to the fault. For the meaning of LTT and DYZ, see more details in the text.

Table 2
CO degassing fluxes of the basins in the BRPB.

Basin	Faults in the basin	Basin length (km)	Basin width (km)	CO degassing		CO uptake		Net CO degassing	
				Flux ($\text{mg m}^{-2} \text{d}^{-1}$)	Amounts ($\times 10^3 \text{ ton/a}$)	Flux ($\text{mg m}^{-2} \text{d}^{-1}$)	Amounts ($\times 10^3 \text{ ton/a}$)	Flux ($\text{mg m}^{-2} \text{d}^{-1}$)	Amounts ($\times 10^3 \text{ ton/a}$)
I	F1	96	30	18.05	19.0	-6.02	-6.3	12.03	12.7
II	F3	78	20	10.62	6.0	n.n.	n.n.	10.62	6.0
III	F2, F4, F5	100	30	6.11	6.7	-4.09	-4.5	2.01	2.2
IV	F6	26	16	0.80	0.1	-23.80	-3.6	-22.9	-3.5
V	F7, F8	50	10	16.82	3.1	-24.37	-4.4	-7.55	-1.4
VI	F9, F10	50	15	3.58	1.0	-52.18	-14.3	-48.6	-13.3
VII	F11	100	16	8.35	4.9	n.n.	n.n.	8.35	4.9

Abbreviations of each basin (from I to VII) and fault (from F1 to F11) correspond to those in Fig. 1(b). Length and width data of each basin are taken from Xu et al. (2002). n.n. = no negative values.

Table 3
Concentrations of CO degassing from soil in the BRPB.

Seismic zone	Measuring site	Fault slip rate (mm/a)	R_c/R_a	CO concentration ($\times 10^{-6}$)
A	1	0.46	1.95	0.53
	2	0.46	1.95	0.56
	3	0.32	0.56	0.7
	4	0.43	0.56	0.49
	5	0.02	n.d.	0.82
	6	n.d.	n.d.	0.57
	7	0.40	n.d.	0.23
	8	0.17	n.d.	0.34
	9	0.34	1.10	0.33
	10	0.24	1.10	0.67
B	11	0.22	n.d.	0.46
	12	0.22	n.d.	0.40
	13	0.20	n.d.	0.44
	14	0.30	n.d.	0.29
	15	0.55	n.d.	1.90
	16	0.47	n.d.	0.29
	17	0.20	0.66	0.76
	18	0.20	0.66	0.62
	19	0.38	2.08	0.24
	20	0.32	2.08	0.33
	21	0.34	2.08	0.58

A and B represent the Shanxi seismic zone and Zhangjiakou-Bohai seismic zone, respectively. The number of each measuring site (from 1 to 21) corresponds to that in Fig. 1(b). R_c/R_a , the air-corrected $^3\text{He}/^4\text{He}$ ratio, are taken from Zhang et al. (2016). n.d. = no data. Data sources of the fault slip rates are as follows: Xu et al. (2002), Zhang et al. (2016), and Fang et al. (1994).

Fiebig et al., 2007; Liu et al., 2010).



5.2. A possible link of CO concentration to the tectonic stress field

Emission of gases from active fault zones, especially from structurally weak zones, can be enhanced by the action of tectonic stress (Du et al., 2008; Toutain and Baubron, 1999). The tectonic stress field is heterogeneous in the BRPB (Zhang et al., 2009a). The local NNW-SSE extensional stress is more distinct in the Shanxi seismic zone in the west of the BRPB (Fig. 1b, Zhang et al., 2009a). The tectonic stress is

characterized by ENE-WSW compressional stress in the Zhangjiakou-Bohai seismic zone (Fig. 1b, Zhang et al., 2009a). A positive correlation ($r = 0.48$) between CO concentration in soil gas and fault slip rate exists in the Zhangjiakou-Bohai seismic zone in the east of the BRPB, whereas the correlation in the Shanxi seismic zone in the west of the BRPB is negative ($r = -0.43$) (Table 3). Deformation in the vicinity of faults suggests that the effective porosity of the normal faults tends to increase through the opening of cracks during interseismic extension (Muir-Wood and King, 1993). The negative correlation between CO concentration in soil gas and fault slip rate in the Shanxi seismic zone might indicate the opening of the normal fault increases the oxygen fugacity in the fault (Fig. 7a) and change characteristics of fluids in the fault from a $\text{CH}_4\text{-H}_2\text{-CO}$ system to a $\text{CO}_2\text{-CO}$ system (Zhang and Duan, 2009; Liu et al., 2010).

Study on the Basin and Range province of the United States indicates that shearing might twist the regional strain and generate vertical faults that link the brittle upper crust with the ductile lower crust (Hilton, 2007). Fluid pressure, which favors the upward migration of gases along fault zones, is greater in strike-slip faults than in normal faults (Sibson, 1996). There are many strike-slip faults (e.g., F7, F8, and F11) in the Zhangjiakou-Bohai seismic zone in the eastern part of the BRPB (Zhang et al., 2009a; Xu et al., 2002). The high slip rate might enhance the compressional stress whereas the low oxygen fugacity favors the generation of CO (Fig. 7b).

CO concentration in soil gas along the active fault zones might be an indicator of the stress field, as suggested by the relationship between CO concentration in soil gas and stress field in the BRPB (Fig. 7). The relationship of CO anomalies and certain earthquakes might be the response to stress variations before, during or after earthquakes (Singh et al., 2010; Cui et al., 2013; Sun et al., 2014).

6. Conclusions

- (1) Concentrations of CO degassing from soil in the BRPB varied between 0.29×10^{-6} and 1.1×10^{-6} . The background value of 0.6×10^{-6} in fault zones was twice the CO concentration in the atmosphere. Net CO fluxes from soil to atmosphere ranged from $-48.6 \text{ mg m}^{-2} \text{d}^{-1}$ to $12.03 \text{ mg m}^{-2} \text{d}^{-1}$. The total amount of CO diffusion in the BRPB was estimated to be as high as $7.6 \times 10^3 \text{ ton/a}$, which is comparable to the output of $1.2 \times 10^4 \text{ ton/a}$ for CO_2 .
- (2) CO concentrations of soil gas in the BRPB varied in spatial. High values of CO concentrations occurred along NE-SW trending, which coincided with low-velocity anomalies and high conductivity in the mantle and high Poisson's ratios in the crust. This indicated that CO in soil gas is partially mantle-derived fluids. Other sources of CO in the soil gas are mainly from chemical reactions among the deep fluids (e.g., oxidation of CH_4 and reduction of CO_2 in $\text{CH}_4\text{-CO}_2\text{-H}_2\text{O}$ fluids) and carbonate minerals (dolomite, limestone, and siderite) in country rocks. Biogenic process may also be a contributor to the CO in soil gas in the BRPB.

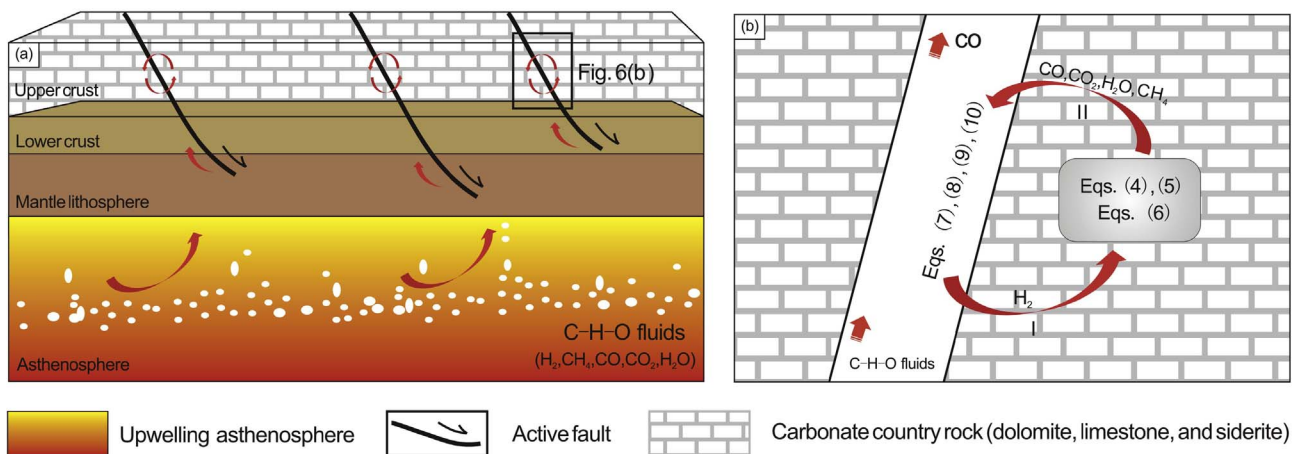


Fig. 6. Illustrations showing generation processes of CO by chemical reactions in the BRPB. (a) Upwelling of asthenospheric mantle releases fluids and volatiles (CH₄, H₂, H₂O, CO, etc.) as well as heat from the deep sources. Deep faults (e.g., the Huailai-Lingqiu, Tianzhen, and Zhuolu-Yangyuan faults, Xu et al., 2002) can act as conduits for migration of the mantle-derived volatiles. Heat from the mantle favors release of CO₂-rich fluids from the carbonates at temperatures above 500 °C (Sulem and Famin, 2009; Santosh et al., 2010). Thermal decomposition of the carbonate rocks [(Mg, Ca)CO₃] and carbon-containing mineral siderite (FeCO₃) may generate CO₂ and CO by Eqs. (4) and (5) in the text (Gao, 1997; Treiman, 2003; McCollom, 2003; Etiope and Lollar, 2013). The volatiles from the upwelling of asthenosphere can react with the carbonate rock (CaCO₃) by Eq. (6) in the text. (b) CO could be generated by chemical reactions among the CO₂-CH₄-H₂-H₂O fluids and by the reactions between the fluids and carbonate country rock by Eqs. (7)–(10) in the text. The fluids can migrate between the fault and the country rock (I and II in Fig. 6b).

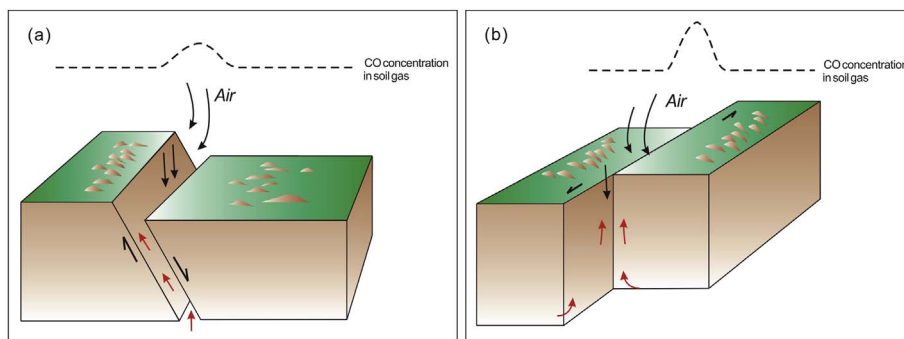


Fig. 7. Schematic model showing stress field related to CO degassing in a normal fault (a) and in a strike slip fault (b). (a) Activities of the normal faults under tectonic stress might increase oxygen fugacity within the fault. CO concentrations across the normal fault are lower than those across the strike slip fault. (b) The fluid pressure in the strike slip fault is greater than that in the normal fault (Sibson, 1996), which favors upward migration of gases along the fault zones. The low oxygen fugacity favors the generation of CO.

(3) CO concentrations in soil gas were influenced by the permeability of fault zones. The spatial variations of CO concentrations in soil gas were related to the changes in the crustal stress field in the BRPB. It can be inferred that CO in soil gas may be an indicator of the crust stress field and seismic activity.

Acknowledgements

This work was funded by the National Natural Science Foundation of China (41673106, 41373059, 41572321, and 41020124002), the CEA Key Laboratory of Earthquake Prediction (2014IES010202, 2016IES010304) and the Key Research Project of Frontier Sciences of Chinese Academy of Sciences (QYZDY-SSW-DQC030). The authors are like to thank John Saul for improving the English and Ziguang Zhang, Yanrui Sheng, Yueling Zhou and Zhihua Ding at the Seismological Bureau of Hebei Province and Yongmei Liu of the Seismological Bureau of the Inner Mongolia Autonomous Region for the help in field measurement. China Earthquake Networks Center provided archived earthquake data for the region. We are grateful to the three anonymous reviewers for their constructive comments to the manuscript.

References

- Agosta, F., Prasad, M., Aydin, A., 2007. Physical properties of carbonate fault rocks, fucino basin (Central Italy): implications for fault seal in platform carbonates. *Geofluids* 7, 19–32.
- Badr, O., Probert, S.D., 1994. Carbon-monoxide concentration in the Earth's atmosphere. *Appl. Energy* 49, 99–143.
- Bergman, S.C., Dubessy, J., 1984. CO₂-CO fluid inclusions in a composite peridotite xenolith: implications for upper mantle oxygen fugacity. *Contrib. Miner. Petrol.* 85, 1–13.
- Chiodini, G., Cioni, R., Guidi, M., Raco, B., Marini, L., 1998. Soil CO₂ flux measurements in volcanic and geothermal areas. *Appl. Geochem.* 13, 543–552.
- Conrad, R., Seiler, W., 1980. Role of microorganisms in the consumption and production of atmospheric carbon monoxide by soil. *Appl. Environ. Microbiol.* 40, 437–445.
- Conrad, R., Seiler, W., 1982. Arid soils as a source of atmospheric carbon monoxide. *Geophys. Res. Lett.* 9, 1353–1356.
- Conrad, R., Thauer, R.K., 1983. Carbon monoxide production by *Methanobacterium thermoautotrophicum*. *FEMS Microbiol. Lett.* 20, 229–232.
- Constant, P., Poissant, L., Villemur, R., 2008. Annual hydrogen, carbon monoxide and carbon dioxide concentrations and surface to air exchanges in a rural area (Québec, Canada). *Atmos. Environ.* 42, 5090–5100.
- Crutzen, P.J., Zimmermann, P.H., 1991. The changing photochemistry of the troposphere. *Tellus* 43, 136–151.
- Cui, Y.J., Du, J.G., Zhang, D.H., Sun, Y.T., 2013. Anomalies of total column CO and O₃ associated with strong earthquakes in recent years. *Nat. Hazards Earth Syst. Sci.* 13, 2513–2519.
- Du, J.G., Si, X.Y., Chen, Y.X., Fu, H., Jian, C.L., Guo, W.S., 2008. Geochemical anomalies connected with great earthquakes in China. In: Stefansson, O. (Eds.), *Geochemistry Research Advances*, New York, pp. 57–92.
- Elio, J., Ortega, M.F., Mazadiego, L.F., Nisi, B., Vaselli, O., Garcia-Martinez, M.J., 2016. Monitoring of soil gases in the characterization stage of CO₂ storage in saline aquifers and possible effect of CO₂ leakage in the groundwater system. In: Vishal, V., Singh, T. N. (Eds.), *Geologic carbon sequestration*, Switzerland, pp. 81–95.
- Etiope, G., Lollar, B.S., 2013. Abiotic methane on Earth. *Rev. Geophys.* 51, 276–299.
- Fan, W., 2015. Geological features and research progress of the Mesoproterozoic Xiamaling formation in the North China Craton: a review after nearly one hundred years of study. *Geol. Rev.* 61, 1383–1406 (in Chinese with English abstract).
- Fang, Z., Duan, R., Zheng, B., Yang, Z., 1994. Research on activity of the northern margin fault of the Huaian basin in Hebei province. *North China Earthquake Sci.* 12, 25–33 (in Chinese with English abstract).

- Fiebig, J., Woodland, A.B., Spangenberg, J., Oschmann, W., 2007. Natural evidence for rapid abiogenic hydrothermal generation of CH₄. *Geochim. Cosmochim. Acta* 71, 3028–3039.
- Frost, D.J., McCammon, C.A., 2008. The redox state of Earth's mantle. *Annu. Rev. Earth Planet. Sci.* 36, 389–420.
- Funk, D.W., Pullman, E.R., Peterson, K.M., Crill, P.M., Billings, W.D., 1994. Influence of water table on carbon dioxide, carbon monoxide, and methane fluxes from taiga bog microcosms. *Global Biogeochem. Cycles* 8, 271–278.
- Gao, P., 1997. Study on the origin of low velocity and high conductivity layer (body) in North China. *Earthquake Res. China* 13, 223–231 (in Chinese with English abstract).
- Gao, Y., Wu, J., Fukao, Y., Shi, Y.T., Zhu, A.L., 2011. Shear wave splitting in the crust in North China: stress, faults and tectonic implications. *Geophys. J. Int.* 187, 642–654.
- Gillenwater, M., Kristina, S., Ajavon A.N., 2006. Chapter 7: Precursors and Indirect Emissions. In: Smith K.A. (Eds.), 2006 IPCC Guidelines for National Greenhouse Gas Inventories, pp. 1–16.
- Gödde, M., Meuser, K., Conrad, R., 2000. Hydrogen consumption and carbon monoxide production in soils with different properties. *Biol. Fertil. Soils* 32, 129–134.
- Hilton, D.R., 2007. The leaking mantle. *Science* 318, 1389–1390.
- Hilton, D.R., Fischer, T.P., Marty, B., 2002. Noble gases and volatile recycling at subduction zones. *Rev. Mineral. Geochem.* 47, 319–370.
- Huang, J.L., Zhao, D.P., 2004. Crustal heterogeneity and seismotectonics of the region around Beijing, China. *Tectonophysics* 385, 159–180.
- Huang, J.L., Zhao, D.P., 2006. High-resolution mantle tomography of China and surrounding regions. *J. Geophys. Res.: Solid Earth* 111, B09305–B09326.
- Huang, J.L., Zhao, D.P., 2009. Seismic imaging of the crust and upper mantle under Beijing and surrounding regions. *Phys. Earth Planet. Inter.* 173, 330–348.
- Kasichke, E.S., Hyer, E.J., Novelli, P.C., Bruhwiler, L.P., French, N.H.F., Sukhinin, A.I., Hewson, J.H., Stocks, B.J., 2005. Influence of boreal fire emissions on Northern Hemisphere atmospheric carbon and carbon monoxide. *Global Biogeochemical Cycles* 19, GB1012–GB1018.
- Khalil, M.A.K., Rasmussen, R.A., Wang, M.X., Ren, L., 1990. Emissions of trace gases from Chinese rice fields and biogas generators: CH₄, N₂O, CO, CO₂, chlorocarbons and hydrocarbons. *Chemosphere* 20, 207–226.
- Lashof, D.A., Ahuja, D.R., 1990. Relative contributions of greenhouse gas emissions to global warming. *Nature* 344, 529–531.
- Li, B., Havskov, J., Ottemöller, L., Sorensen, M.B., 2015. New magnitude scales M_L and spectrum-based M_W for the area around Shanxi Rift System, North China. *J. Seismol.* 19, 141–158.
- Lei, J.S., 2012. Upper-mantle tomography and dynamics beneath the North China Craton. *J. Geophys. Res.: Solid Earth* 117, B06313–B06342.
- Li, Y., Du, J.G., Wang, X., Zhou, X.C., Xie, C., Cui, Y.J., 2013. Spatial variations of soil gas geochemistry in the Tangshan area, Northern China. *Terr., Atmos. Ocean. Sci.* 24, 323–332.
- Liu, J.Q., Chen, L.H., Ni, P., 2010. Fluid/melt inclusions in Cenozoic mantle xenoliths from linqu, Shandong Province, eastern China: implications for asthenosphere-lithosphere interactions. *Chin. Sci. Bull.* 55, 1067–1076.
- Lu, S., Zhao, G., Wang, H., Hao, G., 2008. Precambrian metamorphic basement and sedimentary cover of the North China Craton: a review. *Precamb. Res.* 160, 77–93.
- Lupton, J.E., 1983. Terrestrial inert gases isotope tracer studies and clues to primordial components in the mantle. *Annu. Rev. Earth Planet. Sci.* 11, 371–414.
- McCammon, C., Kopylova, M.G., 2004. A redox profile of the Slave mantle and oxygen fugacity control in the cratonic mantle. *Contrib. Miner. Petrol.* 148, 55–68.
- McCullom, T.M., 2003. Formation of meteorite hydrocarbons from thermal decomposition of siderite (FeCO₃). *Geochim. Cosmochim. Acta* 67, 311–317.
- Menzies, M., Xu, Y., Zhang, H., Fan, W., 2007. Integration of geology, geophysics and geochemistry: a key to understanding the North China Craton. *Lithos* 96, 1–21.
- Nakano, T., Sawamoto, T., Morishita, T., Inoue, G., Hatano, R., 2004. A comparison of regression methods for estimating soil-atmosphere diffusion gas fluxes by a closed-chamber technique. *Soil Biol. Biochem.* 36, 107–113.
- Novelli, P.C., Steele, L.P., Tans, P.P., 1992. Mixing ratios of carbon monoxide in the troposphere. *J. Geophys. Res.: Atmospheres* 97, 20731–20750.
- Prather, M., Ehalt, D., Dentener, F., Derwent, R., Dlugokencky, E., Holland, E., Isaksen, I., Katima, J., Kirchhoff, V., Matson, P., Midgley, P., Wang, M., 2001. Chapter 4: Atmospheric chemistry and greenhouse gases. In: Houghton, J.T., Ding, Y., Griggs, D.J., Noguer, M., van der Linden, P.J., Dai, X., Maskell, K., Johnson, C.A. (Eds.), *Climate Change 2001: The Scientific Basis. Contribution of working group 1 to the third assessment report of the Intergovernmental Panel on Climate Change*, Cambridge, pp. 239–287.
- Ran, Y.K., 1997. Detailed research of paleoearthquakes at several typical regions in China and exploration of recurrence behavior of large earthquakes. Doctor thesis of Institute of Geology, China Earthquake Administration, pp. 1–128.
- Santosh, M., Zhao, D., Kusky, T., 2010. Mantle dynamics of the Paleoproterozoic North China Craton: a perspective based on seismic tomography. *J. Geodyn.* 49, 39–53.
- Schlesinger, W.H., 1999. Carbon and agriculture: carbon sequestration in soils. *Science* 284, 2095–2099.
- Scott, H.P., Hemley, R.J., Mao, H., Herschbach, D.R., Fried, L.E., Howard, W.M., Basted, S., 2004. Generation of methane in the Earth's mantle: in situ high pressure-temperature measurements of carbonate reduction. *Proc. Nat. Acad. USA* 39, 14023–14026.
- Sibson, R.H., 1996. Structural permeability of fluid-driven fault-fracture meshes. *J. Struct. Geol.* 18, 1031–1042.
- Sinclair, A.J., 1991. A fundamental approach to threshold estimation in exploration geochemistry: probability plots revisited. *J. Geochem. Explor.* 41, 1–22.
- Singh, R.P., Kumar, J.S., Zlotnicki, J., Kafatos, M.K., 2010. Satellite detection of carbon monoxide emission prior to the Gujarat earthquake of 26 January 2001. *Appl. Geochem.* 25, 580–585.
- Sulem, J., Famin, V., 2009. Thermal decomposition of carbonates in fault zones: slip-weakening and temperature-limiting effects. *J. Geophys. Res.: Solid Earth* 114, B03309.
- Sun, Y.T., Cui, Y.J., Liu, Y.M., Du, J.G., Zhang, W.B., Zhang, G.Y., 2014. Remote sensing anomalies of CO and O₃ related to two giant Sumatra earthquakes occurred in 2004 and 2005. *Rem. Sens. Inform.* 29, 49–56 (In Chinese with English abstract).
- Taylor, W.R., Green, D.H., 1988. Measurement of reduced peridotite-C-O-H solidus and implications for redox melting of the mantle. *Nature* 332, 349–352.
- Tian, Y., Zhao, D., Sun, R., Teng, J., 2009. Seismic imaging of the crust and upper mantle beneath the North China Craton. *Phys. Earth Planet. Inter.* 172, 169–182.
- Toutain, J.P., Baubron, J.C., 1999. Gas geochemistry and seismotectonics: a review. *Tectonophysics* 304, 1–27.
- Treiman, A.H., 2003. Submicron magnetite grains and carbon compounds in martian meteorite ALH84001: inorganic, abiotic formation by shock and thermal metamorphism. *Astrobiology* 3, 369–392.
- Trump, J.E.V., Miller, S.L., 1973. Carbon monoxide on the primitive Earth. *Earth Planet. Sci. Lett.* 20, 145–150.
- Wang, J., Liu, Q.Y., Chen, J.H., Li, S.C., Guo, B., Li, Y., 2009. The crustal thickness and Poisson's ratio beneath the Capital Circle Region. *Chin. J. Geophys.* 52, 57–66 (in Chinese with English abstract).
- Muir-Wood, R., King, G.C.P., 1993. Hydrological signatures of Earthquake strain. *J. Geophys. Res.* 98, 22035–22068.
- Voltattorni, N., Cinti, D., Pizzino, L., Sciarra, A., 2014. Statistical approach for the geochemical signature of two active normal faults in the western Corinth Gulf Rift (Greece). *Appl. Geochem.* 51, 86–100.
- Xu, S., Chen, M., 2012. Design and modeling of non-linear infrared transducer for measuring methane using cross-correlation method. *Measurement* 45, 325–332.
- Xu, X., Ma, X., 1992. Geodynamics of the Shanxi Rift system, China. *Tectonophysics* 208, 325–340.
- Xu, X.W., Wu, W.M., Zhang, X.K., Ma, S.L., Ma, W.T., Yu, G.H., Gu, M.L., Jiang, W.L., 2002. New crustal structure motion and earthquake in capital area, Beijing, pp. 43–104 (in Chinese with English abstract).
- Yonemura, S., Kawashima, S., Tsuruta, H., 2000. Carbon monoxide, hydrogen, and methane uptake by soils in a temperate arable field and a forest. *J. Geophys. Res.: Atmospheres* 105, 14347–14362.
- Zhang, C., Duan, Z.H., 2009. A model for C-O-H fluid in the Earth's mantle. *Geochim. Cosmochim. Acta* 73, 2089–2102.
- Zhang, H.Y., Xie, F.R., Jing, Z.J., 2009a. Research on heterogeneity of the present tectonic field in the basin-and-range province northwest of Beijing. *Chin. J. Geophys.* 52, 3061–3071 (In Chinese with English abstract).
- Zhang, S.H., Zhao, Y., Yang, Z.Y., He, Z.F., Wu, H., 2009b. The 1.35 Ga diabase sills from the northern North China Craton: implications for breakup of the Columbia (Nuna) supercontinent. *Earth Planet. Sci. Lett.* 288, 588–600.
- Zhang, W.B., Du, J.G., Zhou, X.C., Wang, F., 2016. Mantle volatiles in spring gases in the Basin and Range Province on the west of Beijing, China: constraints from helium and carbon isotopes. *J. Volcanol. Geoth. Res.* 309, 45–52.
- Zhou, X.C., Du, J.G., Chen, Z., Cheng, J.W., Tang, Y., Yang, L.M., Xie, C., Cui, Y.J., Liu, L., Yi, L., Yang, P.X., Li, Y., 2010. Geochemistry of soil gas in the seismic fault zone produced by the Wenchuan Ms = 8.0 earthquake, southwestern China. *Geochem. Trans.*, 11, 5.
- Zhou, X.C., Zhi, C., Cui, Y.J., 2015. Environmental impact of CO₂, Rn, Hg degassing from the rupture zones produced by Wenchuan Ms 8.0 earthquake in western Sichuan, China. *Environ. Geochem. Health* 38, 1067–1082.